Griffiths, D. V. (1994). *Géotechnique* **44**, No. 2, 297–305

Seepage beneath unsymmetric cofferdams

D. V. GRIFFITHS*

Finite element analyses have been performed on the problem of two-dimensional groundwater flow beneath cofferdam walls of unequal length. The results indicate that the problem may be idealized as two independent flow systems separated by a vertical line. An optimum location for this line can be found which enables good approximate solutions for flow rates and exit gradients to be obtained.

KEYWORDS: **cut-off walls and barriers; groundwater; numerical modelling and analysis; permeability; seepage; sheet piles and cofferdams.**

Des analyses par éléments finis ont été développées pour des problèmes d'écoulements souterrains bidimensionnels sous des murs coffrés de différentes longueurs. Les résultats obtenus montrent que le problème peut-être assimilé à deux systèmes d'écoulement indépendants séparés par une ligne verticale. La localisation de cette ligne peut-être optimisée. Elle permet d'obtenir des solutions approchées des vitesses d'écoulement et des gradients de sortie satisfaisantes.

INTRODUCTION

One type of double-wall cofferdam encountered in geotechnical engineering is constructed of driven sheet pile walls. Although actually three-dimensional, such systems are often modelled as two-dimensional if they are long relative to their width. Following dewatering between the walls, these structures allow construction or remedial work to be performed on sites that were initially underwater.

Of particular interest to engineers are the overall stability of the soil/wall system, the volumetric flow rate passing through the foundation soils and the exit gradients that might be experienced inside the cofferdam. This Paper addresses the prediction of flow rate and exit gradients; the latter have a significant influence on overall stability.

The traditional method of analysis available to engineers for the prediction of such quantities as flow rates and exit gradients has involved the use of flow nets. This trial and error approach (Casagrande, 1940; Cedergren, 1967) can lead to accurate predictions if the flow net is drawn carefully; however, its use requires much practice and experience.

Analytical methods are available for cofferdams with walls of equal length (e.g. Harr, 1962; Verruijt, 1970; Banerjee & Muleshkov 1992), but this Paper is concerned with the problem of steady seepage through cofferdam walls of unequal length. It is shown that this non-symmetric problem can be solved to a reasonable degree of accuracy by use of existing approximate methods without resort to analytical or numerical analysis. However, finite element solutions have been used to validate the method.

Figure 1 shows the boundary value problem, where L is the distance between the walls, T is the depth of the soil layer, W is the distance to the side boundary, s' is the length of the left wall and s'' is the length of the right wall, which is conveniently expressed in dimensionless form as the wall spacing ratio L/T, the left wall length ratio s'/T and the right wall length ratio s''/T.

At the root of the investigation is the location of the streamline which divides the flow coming from the left and right of the cofferdam, e.g. the thick line in the flow net of Fig. 2.

Under examination in this work is the extent to which the dividing streamline can be idealized as

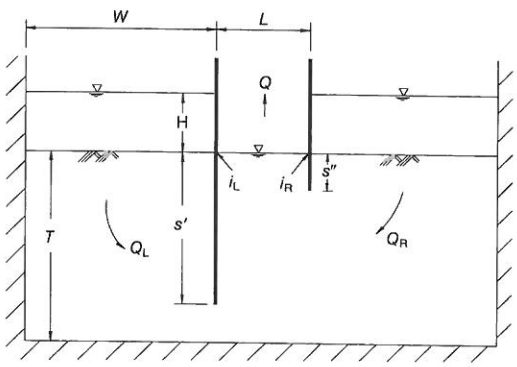

Fig. 1. General layout of unsymmetric cofferdam

Manuscript received 29 March 1993; accepted 8 June 1993.
Discussion on this Paper closes 1 September 1994; for further details see p. ii.
* Colorado School of Mines.

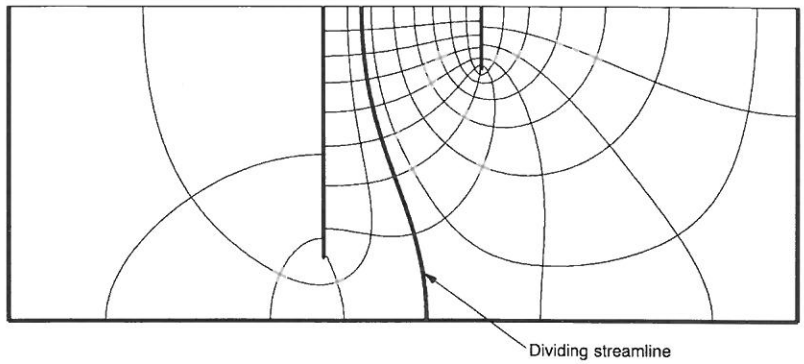

Fig. 2. Location of dividing streamline: $s'/T = 0{\cdot}8$, $L/T = 0{\cdot}5$, $s''/T = 0{\cdot}2$

a vertical line. This idealization would enable flow beneath the left and right walls to be treated as two separate problems with simple boundary conditions. If this approximation is shown to be acceptable, then other powerful approximate techniques, such as the method of fragments (Pavlovsky, 1933; Harr, 1962; Griffiths, 1984) can be employed to find solutions to the unsymmetrical system.

FINITE ELEMENT FORMULATION

A program has been developed to solve Laplace's equation with the boundary conditions indicated in Fig. 1, together with a post-processor for contouring of equipotentials and streamlines. Typical meshes are composed of square four-node quadrilateral elements, all of the same size. To give an indication of the mesh refinement used in this study, the depth dimension T was always discretized using 40 elements. The program enables the dimensions of the problem and the lengths of walls to be altered through the data. Output from the program gives the flow rate beneath the left and right walls Q_L and Q_R together with the two exit gradients i_L and i_R.

The assembly of element conductivity matrices into a global conductivity matrix **K** follows standard finite element methodology (e.g. Smith & Griffiths, 1988); however, as all the elements are square and the same size, the symmetric element conductivity matrices in this study are constant and given by

$$\mathbf{k} = \frac{k}{6}\begin{bmatrix} 4 & -1 & -2 & -1 \\ & 4 & -1 & -2 \\ & & 4 & -1 \\ & & & 4 \end{bmatrix} \tag{1}$$

where k is the (isotropic) soil permeability.

BOUNDARY CONDITIONS

In order to plot the flow net for this problem, both the potential and the streamline problems were solved. The potential problem was solved first, the boundary values being fixed at unity on the upstream surfaces ($H = 1$) and at zero on the downstream surface as shown in Fig. 3.

In all cases, fixed values on the boundaries were prescribed using the stiff-spring technique. In the potential problem, for example, this involves adding a large number to the appropriate diagonal terms of **K** and placing the augmented diagonal term multiplied by the fixed value into the corresponding location in the right-hand-side flow vector $\bar{\boldsymbol{q}}$. This modified set of equations given by

$$\bar{\mathbf{K}}\boldsymbol{\phi} = \bar{\boldsymbol{q}} \tag{2}$$

is then solved for $\boldsymbol{\phi}$ by use of conventional Gaussian elimination.

The nodal flow rates are then retrieved by forming the product of the nodal potential vector $\boldsymbol{\phi}$ with the original (undoctored) global conductivity matrix **K**, thus

$$\mathbf{K}\boldsymbol{\phi} = \boldsymbol{q} \tag{3}$$

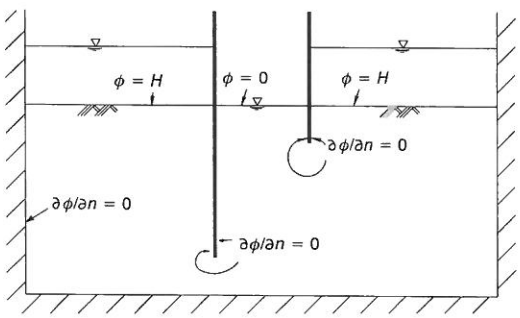

Fig. 3. Boundary conditions for potential problem

The resulting vector $\boldsymbol{q}$ contains zeros at all locations except those corresponding to the fixed freedoms. These non-zero values were simply summed to give the flow rate under the left and right walls Q_L and Q_R respectively. Once these values were found, the streamline problem could be solved by use of the boundary conditions shown in Fig. 4.

Following solution of the potential and stream problems, a post-processor reads the nodal values and contours these two scalar fields. Conventional flow nets try to ensure that the resulting zones between adjacent equipotentials and streamlines are approximately square. This convention affects the size of the contour interval selected for the potentials and streamlines by the plotting program. The square convention is virtually impossible to achieve, however, without an excessive number of flow channels in the unsymmetrical cofferdam. This is because different flow quantities are passing through each side of the system.

The approach used in the present work to select the contour interval was based on the flow-net equation

$$Q = kH(n_f/n_d) \tag{4}$$

where Q is the total flow rate $Q_L + Q_R$, k is the isotropic permeability, H is the total head loss, n_f is the number of flow channels and n_d is the number of equipotential drops. Once Q is computed following the solution of the potential problem, the ratio n_f/n_d follows from equation (4), assuming k and H are known. The number of flow channels n_f is then fixed as a whole number and the number of equipotential drops n_d is computed. In general, n_d will not be a whole number, but is rounded to the nearest integer. This rounding process results in a flow net with some rectangular zones, as occurred in Fig. 2. Alternatively, it will always be possible to find integers n_f and n_d that closely approximate the computed ratio n_f/n_d and therefore result in square zones throughout the flow net. However, this will often involve an excessive number of flow channels for practical purposes.

Figure 4 shows that the maximum and minimum streamline values occur on the cut-off walls themselves, and it is this interval that is divided into n_f flow channels. It would clearly be merely coincidental if one of the contour values coincided with the contour value of zero given to the outer boundary of the flow system. Consequently, the squares are well-defined between the cut-off walls, but tend to become rectangular in the regions of the flow net close to the outer boundary.

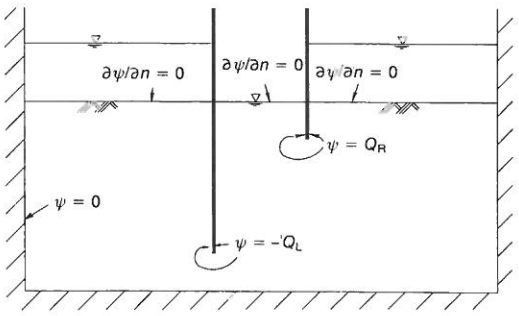

Fig. 4. Boundary conditions for streamline problem

An initial check was made on the effect of the boundary proximity W to the left and right of the walls on computed flow rates and exit gradients. These results are summarized in Table 1 for the case of $s'/T = 0{\cdot}8$, $s''/T = 0{\cdot}2$ and $L/T = 0{\cdot}5$. The results indicate that the boundary effect is insignificant in the present case, with a five-fold increase in the boundary distance changing the flow rate and exit gradients by less than 2%. An alternative means of generating flow nets by the finite element method is discussed by Fan, Tompkins, Drumm & von Bernuth (1992).

Table 1. Effect of boundary distance from walls

Boundary distance W	Q	i_L	i_R
$L + T/2$	0·744	0·297	0·489
$L + T$	0·755	0·302	0·495
$L + 2T$	0·758	0·304	0·496

IDEALIZATION

The extent to which the unsymmetric cofferdam problem can be idealized as two separate flow problems separated by a vertical impermeable barrier, as shown in Fig. 5, is now examined.

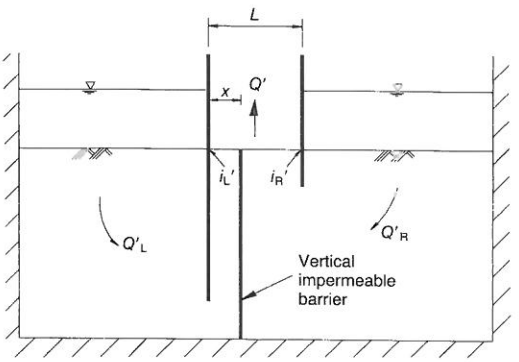

Fig. 5. Idealized flow problem with vertical barrier

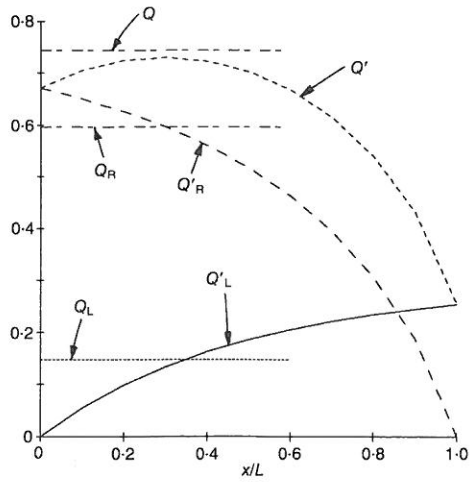

Fig. 6. Influence of barrier position on flow rates: $L/T = 0{\cdot}5$, $s'/T = 0{\cdot}8$, $s''/T = 0{\cdot}2$

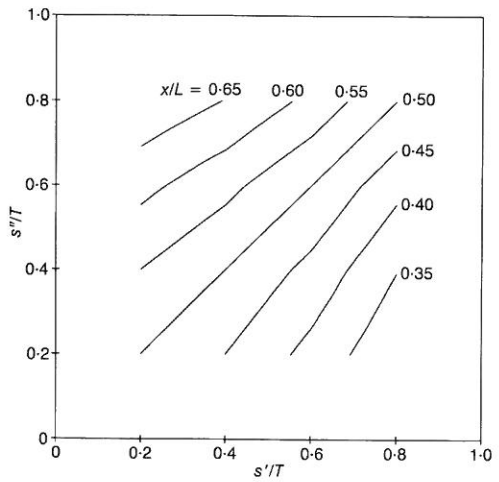

Fig. 7. Optimum barrier position based on flow rates: $L/T = 0{\cdot}5$

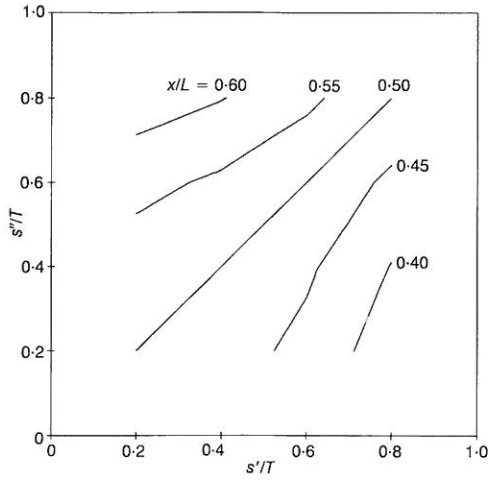

Fig. 8. Optimum barrier position based on flow rates: $L/T = 1{\cdot}0$

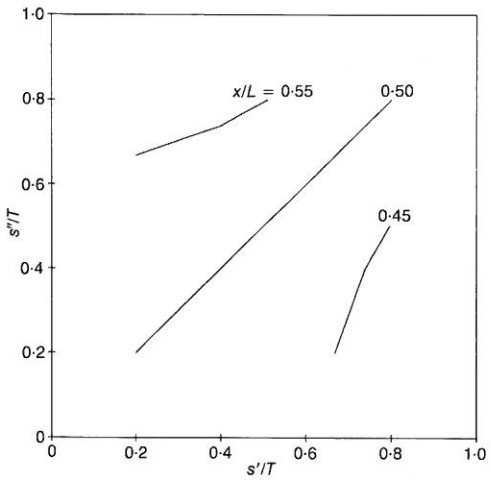

Fig. 9. Optimum barrier position based on flow rates: $L/T = 2{\cdot}0$

Table 2. Optimum values of x/L for $L/T = 0{\cdot}5$ (flow rates)

s''/T	$s'/T = 0{\cdot}2$	$s'/T = 0{\cdot}4$	$s'/T = 0{\cdot}6$	$s'/T = 0{\cdot}8$
0·8	0·691	0·648	0·586	0·500
0·6	0·615	0·565	0·500	0·414
0·4	0·560	0·500	0·435	0·352
0·2	0·500	0·450	0·385	0·309

Table 3. Optimum values of x/L for $L/T = 1{\cdot}0$ (flow rates)

s''/T	$s'/T = 0{\cdot}2$	$s'/T = 0{\cdot}4$	$s'/T = 0{\cdot}6$	$s'/T = 0{\cdot}8$
0·8	0·627	0·602	0·563	0·500
0·6	0·565	0·541	0·500	0·437
0·4	0·525	0·500	0·459	0·398
0·2	0·500	0·475	0·435	0·373

Table 4. Optimum values of x/L for $L/T = 2{\cdot}0$ (flow rates)

s''/T	$s'/T = 0{\cdot}2$	$s'/T = 0{\cdot}4$	$s'/T = 0{\cdot}6$	$s'/T = 0{\cdot}8$
0·8	0·575	0·562	0·560	0·500
0·6	0·537	0·523	0·500	0·460
0·4	0·513	0·500	0·477	0·438
0·2	0·500	0·487	0·463	0·425

In order to find the best position of this barrier, a sequence of calculations was performed in which it was systematically moved across the region between the walls. For each location of the dividing line as defined by the dimensionless ratio x/L, two separate problems were solved, corresponding to the left and right. These analyses yielded the flow rates Q_L' and Q_R' and exit gradients i_L' and i_R' to the left and right; the prime distinguishes these quantities from their counterparts in the original problem. A full parametric study was performed in which the wall lengths were varied in the range

$$0{\cdot}2 \leqslant s'/T,\ s''/T \leqslant 0{\cdot}8$$

and wall spacing was varied in the range

$$0{\cdot}5 \leqslant L/T \leqslant 2{\cdot}0$$

Flow rates

To illustrate the difference between the idealized and original problems, results are presented for the case of $s'/T = 0{\cdot}8$, $s''/T = 0{\cdot}2$, $L/T = 0{\cdot}5$. The plots shown in Fig. 6 give the total flow from the idealized problem defined as

$$Q' = Q_L' + Q_R' \tag{5}$$

and the individual flows from the left and right Q_L' and Q_R' as a function of x/L. Fig. 6 also shows, as horizontal lines, the total flow Q and the flow from the left and right Q_L and Q_R from the original problem.

From Fig. 6, the optimum value of x/L corresponds to the maximum value of the flow Q' where it is closest to the total flow rate from the original problem Q. This is a reminder that, in the original problem, the dividing streamline positions itself so as to optimize the flow rate through the system. In the idealized analyses the maximum value of Q' was always less than Q, although the agreement was generally very good. The case plotted in Fig. 6 gave the worst agreement for all the wall lengths and spacings considered.

This optimum value of x/L is best observed by comparison of the intersection of the horizontal lines representing flow rates from the left and right in the original problem with the corresponding curves from the idealized problem. Tables 2–4 summarize the optimum locations of x/L, based on a weighted average of the left and right flow rates.

The values given in Tables 2–4 are shown in Figs 7–9 respectively. It is clear from these results that the optimum value of x/L is more sensitive to the wall lengths when $L/T = 0{\cdot}5$ than when $L/T = 2{\cdot}0$. In the former case, for the range of wall lengths considered, the optimum value of x/L lies in the range $0{\cdot}35 < x/L < 0{\cdot}65$; in the latter case it lies in the range $0{\cdot}45 < x/L < 0{\cdot}55$. This means that for a wider wall spacing, the optimum location of the dividing line is approximately central irrespective of wall lengths. This interpretation is confirmed by Figs 10 and 11, which compare the dividing streamline, with the optimum location. For the narrowest wall spacing ($L/T = 0{\cdot}5$) given in Fig. 10, the dividing streamline is curved, so the optimum location of $x/L = 0{\cdot}309$ is clearly an approximation. For the widest wall spacing ($L/T = 2{\cdot}0$) shown in Fig. 11,

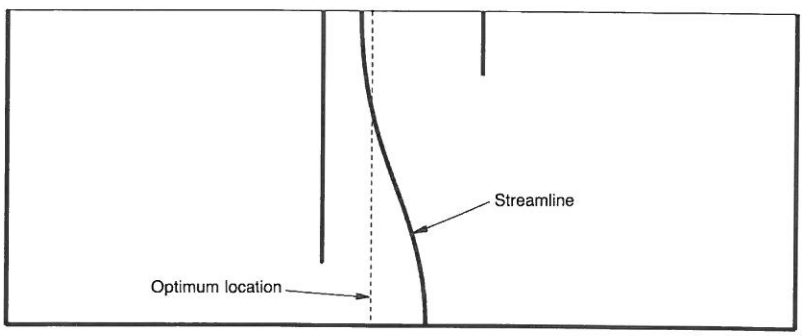

Fig. 10. Actual and idealized dividing lines: $L/T = 0{\cdot}5$, $s'/T = 0{\cdot}8$, $s''/T = 0{\cdot}2$

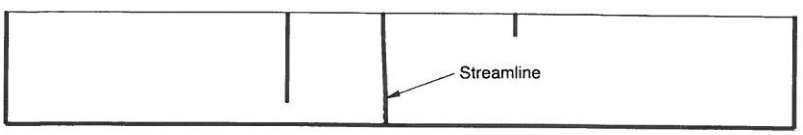

Fig. 11. Actual and idealized dividing lines $L/T = 2{\cdot}0$, $s'/T = 0{\cdot}8$, $s''/T = 0{\cdot}2$

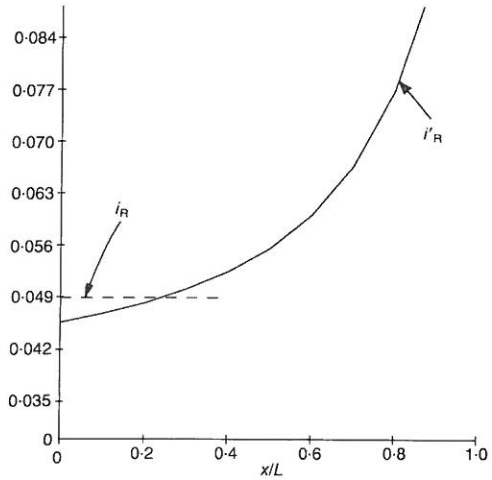

Fig. 12. Influence of barrier position on exit gradient: $L/T = 0{\cdot}5$, $s'/T = 0{\cdot}8$, $s''/T = 0{\cdot}2$

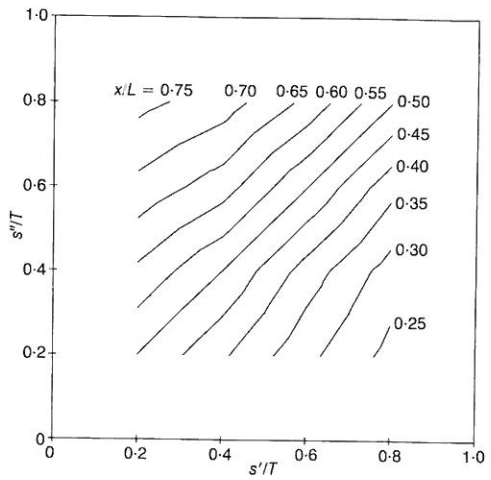

Fig. 13. Optimum barrier position based on exit gradient: $L/T = 0{\cdot}5$

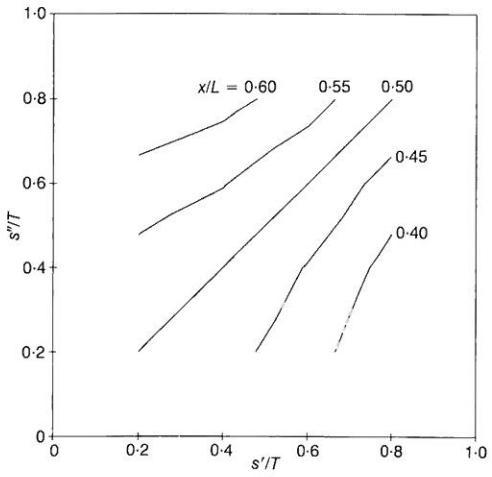

Fig. 14. Optimum barrier position based on exit gradient: $L/T = 1.0$

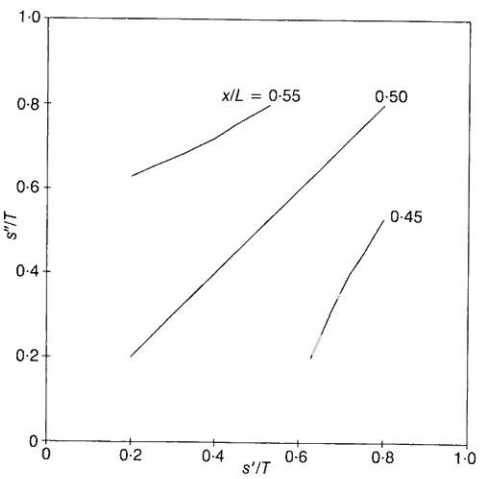

Fig. 15. Optimum barrier position based on exit gradient: $L/T = 2.0$

Table 5. Optimum values of x/L for $L/T = 0{\cdot}5$ (maximum gradient)

s''/T	$s'/T = 0{\cdot}2$	$s'/T = 0{\cdot}4$	$s'/T = 0{\cdot}6$	$s'/T = 0{\cdot}8$
0·8	0·765	0·724	0·635	0·500
0·6	0·686	0·623	0·500	0·365
0·4	0·591	0·500	0·377	0·276
0·2	0·500	0·409	0·314	0·235

Table 6. Optimum values of x/L for $L/T = 1{\cdot}0$ (maximum gradient)

s''/T	$s'/T = 0{\cdot}2$	$s'/T = 0{\cdot}4$	$s'/T = 0{\cdot}6$	$s'/T = 0{\cdot}8$
0·8	0·644	0·617	0·574	0·500
0·6	0·578	0·553	0·500	0·426
0·4	0·532	0·500	0·447	0·383
0·2	0·500	0·468	0·422	0·356

Table 7. Optimum values of x/L for $L/T = 2{\cdot}0$ (maximum gradient)

s''/T	$s'/T = 0{\cdot}2$	$s'/T = 0{\cdot}4$	$s'/T = 0{\cdot}6$	$s'/T = 0{\cdot}8$
0·8	0·586	0·565	0·542	0·500
0·6	0·544	0·527	0·500	0·458
0·4	0·516	0·500	0·473	0·435
0·2	0·500	0·484	0·456	0·414

however, the dividing streamline is itself almost vertical, and is indistinguishable from the optimum location of $x/L = 0{\cdot}425$.

Exit gradients

Figure 12 gives the exit gradient next to the right wall i_R' as a function of x/L for the same case as that considered in Fig. 6. The right wall is chosen because it is the shorter, and hence the wall against which the highest exit gradients would be observed.

Also indicated in Fig. 12 is the value i_R obtained from the original problem. The point of intersection of the lines represents the optimum value of x/L for modelling of the exit gradient. Tables 5–7 summarize the results for all the cases considered; Figs 13–15 summarize them for the range of wall lengths considered. As the values given in these plots are based on optimization of the accuracy of the maximum exit gradient, this could correspond to the left or the right wall, depending on the values of s'/T and s''/T.

These results indicate that the optimum value of x/L is more sensitive to wall length variations in the prediction of exit gradients than in the prediction of flow rates. This is because the exit gradient is a derivative whereas the flow rate is an integral, the latter being an inherently more stable process numerically. The difference is most pronounced for smaller wall spacing. The following examples correspond to two different wall spacings, but with the same wall lengths given by $s'/T = 0{\cdot}8$ and $s''/T = 0{\cdot}2$.

(*a*) When $L/T = 0{\cdot}5$, the optimum x/L is 0·309 (based on flow rate) and 0·235 (based on maximum exit gradient).
(*b*) When $L/T = 2{\cdot}0$, the optimum x/L is 0·425 (based on flow rate) and 0·414 (based on maximum exit gradient).

Figures 7 and 13 differ significantly, and for lesser wall spacings it may be justified to solve the flow and exit gradient problems using two different x/L values such as those given in (*a*). However, the optimum value of x/L based on flow rates will tend to give an overestimate (conservative) of the maximum exit gradient; the optimum value of x/L based on the maximum exit gradient will tend to give a further underestimate (unconservative) of the total flow rate. Figs 8 and 14 are similar, and Figs 9 and 15 are substantially the same, indicating that for larger wall spacing a single idealization for both flow and exit gradients will certainly be sufficient, as confirmed by (*b*).

Although the different values of x/L indicated for the lesser wall spacings are unlikely to affect the final calculation of flow rate and exit gradients significantly, the optimum values from flow rate considerations are recommended if a single idealization is to be used.

EXAMPLE

To demonstrate the method described, a simple example is now presented. With reference to the problem definitions given in Fig. 1, a cofferdam with $L/T = 1$, $s'/T = 0{\cdot}8$, $s''/T = 0{\cdot}2$ and $s'' = 8$ is considered. The flow net and results generated by the finite element analysis are shown in Fig. 16.

From Table 3, the optimal location of a vertical barrier based on flow rates is given by $x/L = 0{\cdot}373$. From the method of fragments and Figs 17 and 18 given by Griffiths (1984), the normalized flow rate is

$$\bar{Q} = \frac{Q}{kH} = \frac{1}{\Sigma\Phi} \tag{6}$$

(from equation (4), $\Sigma\Phi = n_d/n_f$). From Fig. 17, the flow through the left side of the problem is

$$\sum \Phi = 1{\cdot}62 + 2{\cdot}75 \tag{7}$$

Hence

$$\bar{Q}_L = 0{\cdot}23 \tag{8}$$

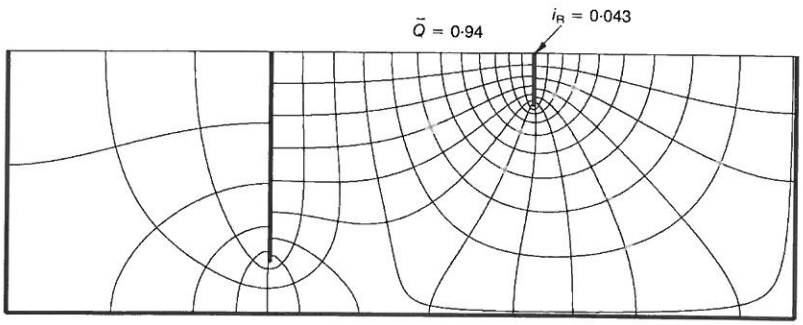

Fig. 16. Computed flow net for example problem

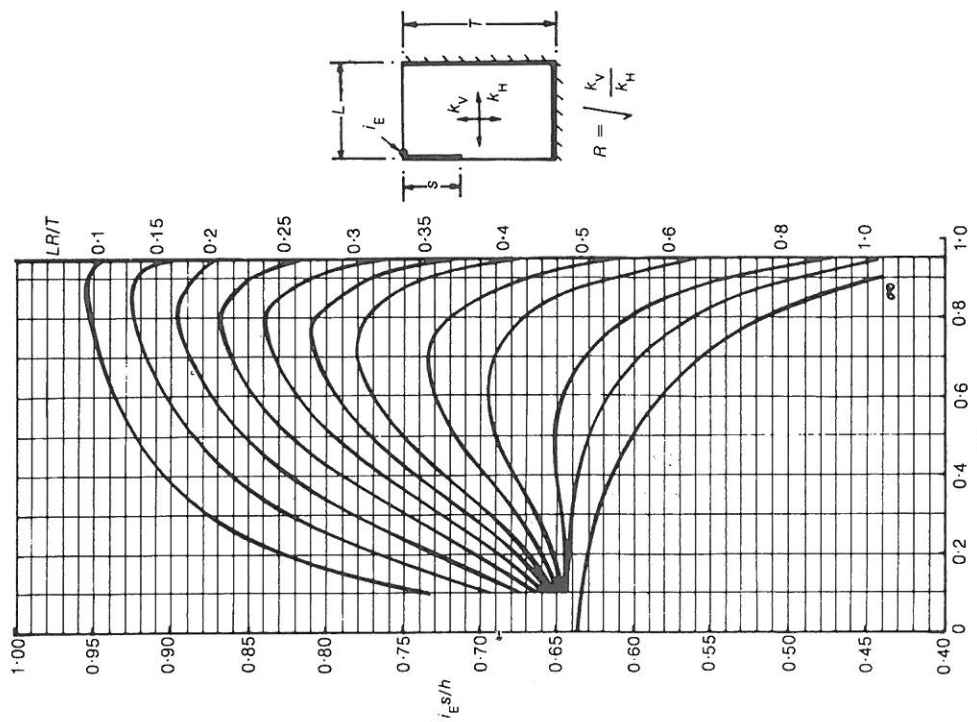

Fig. 18. Chart for obtaining the exit gradient

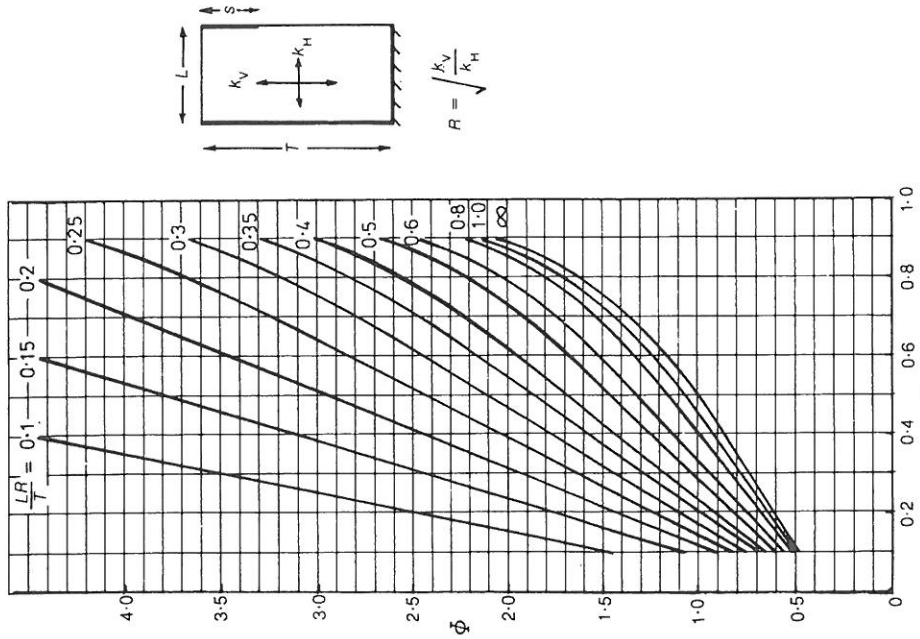

Fig. 17. Chart for obtaining the form factor

and, through the right side of the problem

$$\sum \Phi = 0{\cdot}73 + 0{\cdot}61 \tag{9}$$

Hence

$$\bar{Q}_R = 0{\cdot}75 \tag{10}$$

Thus, by the method of fragments, the total normalized flow is given approximately by

$$\bar{Q} = 0{\cdot}98 \tag{11}$$

which is comparable with 0·94 from the finite element analysis.

The exit gradient against the shortest wall can also be estimated from Fig. 18 in the form

$$i_e s/h = 0{\cdot}65 \tag{12}$$

where

$$s = 8$$

$$h = 0{\cdot}73/(0{\cdot}73 + 0{\cdot}61) = 0{\cdot}54$$

Hence

$$i_e = 0{\cdot}044 \tag{13}$$

which is comparable with 0·043 from the finite element analysis.

CONCLUSIONS

The Paper addresses the problem of steady seepage in two dimensions beneath unsymmetric cofferdams. The main items of interest are the total flow rate through the system and the maximum exit gradient. Parametric studies were performed in which the wall lengths and spacing were systematically varied. For the range of parameters considered, it is shown that the system can be idealized to a reasonable degree of accuracy as two independent flow problems separated by a vertical impermeable barrier. Optimum locations for the barrier are presented as a function of the wall lengths and spacing. The simplified approach based on the superposition of two flow systems with simple geometry makes the problem amenable to powerful approximate solution methods such as the method of fragments.

The idealization is least accurate for small wall spacings (when the true dividing streamline is most curved), and most accurate for large wall spacings (when the true dividing streamline is almost vertical).

The location of the barrier in the idealized problem differed when the flow rate and the exit gradient were being optimized: the former was always more centrally located between the walls. The difference was more apparent for small wall spacings and negligible for large wall spacings. The optimum value based on the flow rate would be the most conservative choice if a single idealization were to be performed.

NOTATION

h	head lost in fragment
H	head difference across dam
i_e	exit gradient (Griffiths, 1984)
i_L, i_R	exit gradients from full analysis
i_L', i_R'	exit gradients from idealized analysis
k	permeability (isotropic)
$\mathbf{k}$	element conductivity matrix
$\mathbf{K}$	global conductivity matrix
$\bar{\mathbf{K}}$	modified global conductivity matrix
L	distance between walls
n_d, n_f	number of equipotential drops and flow channels
$\boldsymbol{q}$	nodal flow vector
$\bar{\boldsymbol{q}}$	modified nodal flow vector
Q, Q_L, Q_R	flow rates from full analysis
Q', Q_L', Q_R'	flow rates from idealized analysis
$\bar{Q}$	normalized flow rate
s, s', s''	wall lengths
T	soil depth
W	distance to side boundary
x	position of vertical barrier
ϕ	potential function
Φ	form factor
ψ	stream function

REFERENCES

Banerjee, S. & Muleshkov, A. (1992). Analytical solution of steady seepage into double-walled coffer-dams. *J. Engng Mech. Div. Am. Soc. Civ. Engrs* **118**, No. 3, 59.

Casagrande, A. (1940). *Seepage through dams.* Boston Society of Civil Engineers.

Cedergren, H. R. (1967). *Seepage, drainage and flow nets.* Chichester: Wiley.

Fan, Y., Tompkins, F. D., Drumm, E. C. & von Bernuth, R. D. (1992). Generation of flow nets using FEM nodal potentials and bilinear shape of functions. *Int. J. Numer. Anal. Methods Geomech.* **16**, No. 6, 425–437.

Griffiths, D. V. (1984). Rationalized charts for the method of fragments applied to confined seepage. *Géotechnique* **34**, No. 2, 229–238.

Harr, M. E. (1962). *Groundwater and seepage.* London: McGraw-Hill.

Pavlovsky, N. N. (1933) Motion of water under dams. *Proc. 1st Congr. Large Dams, Stockholm*, 179–192.

Smith, I. M. & Griffiths, D. V. (1988). *Programming the finite element method*, 2nd edn. Chichester: Wiley.

Verruijt, A. (1970). *Theory of groundwater flow.* London: Macmillan.